Experimental study of the wall-mounted cylinder wake effects on a tidal turbine behaviour compared to free stream turbulence

Maria Ikhennicheu, Benoît Gaurier, Grégory Germain, Philippe Druault, Grégory Pinon, Jean-Valery Facq

Experimental study of the wall-mounted cylinder wake effects on a tidal turbine behaviour compared to free stream turbulence

Maria Ikhennicheu*, Benoît Gaurier*, Grégory Germain*, Philippe Druault†, Grégory Pinon‡, Jean-Valéry Facq *
*Marine Structure Laboratory, IFREMER, 150 Quai Gambetta, 62200 Boulogne sur Mer. France
E-mail: gregory.germain@ifremer.fr
†Sorbonne Université, UPMC Univ Paris 06, CNRS, UMR 7190, Institut Jean Le Rond d'Alembert, F-75005 Paris, France
E-mail: philippe.druault@sorbonne-universite.fr
‡LOMC-UMR 6295, Normandie Univ, UNIHAVRE, CNRS, 76600 Le Havre, France
E-mail: gregory.pinon@univ-lehavre.fr

***Abstract*—Turbulence impacts significantly the performance and fatigue of tidal turbines. In this study, two cases of turbulence inflows are considered. At laboratory scale, in the wave and current circulating tank of Ifremer, experimental conditions are chosen to be representative of *in-situ* characteristics at a 1:20 scale, in Froude similitude ($F_r = 0.23$ and $R_e \sim 10^5$). The first inflow case is seabed variations, experimentally represented with a wall-mounted cylinder. Recent experiments have shown that a large aspect ratio bottom-mounted obstacle produces a very extended wake, with large velocity fluctuations. The second inflow case is a 14% ambient turbulence intensity flow. The main objective of this study is to characterize the effect of the turbulence present in the two inflow cases on a 3-bladed horizontal turbine. The turbine is positioned within the obstacle wake at a distance of $16H$ from the obstacle or within the ambient turbulent flow. To monitor the velocity fluctuations reaching the turbine, two types of measurement are performed in synchronisation with the turbine parameters: Particle Image Velocimetry (PIV) and Laser Doppler Velocimetry (LDV). Measurements are performed far upstream and close to the turbine. In this work, both inflow conditions will be spatially and temporally described. Then, a full temporal and spectral analysis will be achieved on the turbine performance, in terms of thrust and torque. Finally, a comparison will be proposed, between the perturbation effects on the turbine induced by both inflow cases.**

***Index Terms*—Turbulence, Horizontal Axis Tidal Turbine, Experimental trials, wall-mounted cylinder, LDV, PIV**

I. Introduction

For the past ten years, high level of turbulence have been measured in tidal stream sites [Thomson et al., 2012, Sellar et al., 2018]. In France, the Alderney Race is one of the most energetic location with a high turbulence rate in the entire water column, originating mainly from large bathymetry variations [Myers and Bahaj, 2005]. This turbulence can affect significantly the performance and fatigue of tidal turbines [Duràn Medina et al., 2017, Mycek et al., 2014]. In [Ikhennicheu et al., 2018, Ikhennicheu et al., 2019], experiments are performed on bathymetry elements representing the area of interest for tidal turbine applications, with a mean variation of $5m$ at full scale. These elevations are experimentally represented by a unitary wall-mounted square cylinder. Recent experimental results showed that an isolated large aspect ratio wall-mounted square cylinder produces a very extended wake and large velocity fluctuations. Some of these energetic structures are able to rise up to the surface and to generate boils at the free surface. These events are described in [Best, 2005] and are formed in the specific case of large aspect ratio obstacles [Diabil et al., 2017]. Such large events can have the turbine size and are likely to have a significant impact on them if positioned in the obstacle wake. The case of a turbine immersed in an obstacle wake submitted to large energetic turbulent events must be investigated.

Other *in-situ* sites display a high turbulence intensity not only coming form the seabed but rather spread all over the flow due to coastal effects. *In-situ*, turbulence intensity can vary between $[3\%; 24\%]$ [Mycek et al., 2014]. The impact of ambient turbulence intensity on tidal turbines has already been investigated in various papers. [Mycek et al., 2014] underline the effect of turbulence intensity on the turbine wake, [Duràn Medina et al., 2017] on their power production and [Davies et al., 2013] on their fatigue. In high turbulence intensity areas, large turbulent structures can be observed, although they do not originate in any obstacle wake [Duràn Medina et al., 2017]. This case of a high turbulence intensity flow impacting the turbine must also be discussed.

This paper proposes to compare these two kinds of incoming turbulent flows and to investigate their impact on the tidal turbine loads through spatial, temporal and spectral analysis. Such an analysis was initiated in the works of [Kelley et al., 2005] on wind turbines, where 3 cases of turbulent inflow fields are considered with or without coherent structures. They explain the resonant coupling of energy between coherent turbulent fields and the natural vibrational modes of the wind turbine rotor blade as coherent turbulent structures pass. [Chamorro et al., 2015, Chamorro et al., 2014] also investigated the impact of vertical cylinder Von-Kármán vortices on a turbine. They showed the dependency of the

spectral response of the turbine power on the turbulent fluctuations.

In this paper, the experimental set-up is first described. Then, both incoming flow cases *i.e.* a low turbulence intensity flow with the presence of a large wall-mounted obstacle and a high ambient turbulent flow without any obstacle, are described. The impacts of these two flow conditions on an experimental tidal turbine are investigated and then compared.

This work is partly done under the Interreg 2 Seas Met-Certified project [Germain et al., 2018]. Hence, a special attention has been paid on how to take into account and measure the incoming flow in order to properly compute the tidal turbine performances.

II. Experimental set-up

A. The IFREMER flume tank

Tests have been carried out in the wave and current circulating flume tank of IFREMER located in Boulogne-sur-Mer (France) presented in figure 1. The test section is $18m$ long $\times$ $4m$ wide $\times$ $2m$ deep and the incoming flow is assumed to be steady and uniform. Turbulence intensity I in the incoming flow is defined in equation 1, where σ stands for standard deviation. The free stream turbulence in the tank is $I = 14\%$ [Gaurier et al., 2018b]. By means of a grid combined with a honeycomb (that acts as a flow straightener) placed at the inlet of the working section (see fig. 1(a)), a low turbulent intensity of $I = 1.5\%$ is achieved.

$$I_{3D} = I = 100\sqrt{\frac{\frac{1}{3}[\sigma(u_\infty)^2 + \sigma(v_\infty)^2 + \sigma(w_\infty)^2]}{\overline{u_\infty}^2 + \overline{v_\infty}^2 + \overline{w_\infty}^2}} \quad (1)$$

The three instantaneous velocity components are denoted (U, V, W) along the (X, Y, Z) directions respectively (see fig.2). Each instantaneous velocity component is separated into a mean value and a fluctuation part, according to the Reynolds decomposition: $U = \overline{U} + u'$, where an overbar indicates the time average. In the following, non dimensional lengths are used for all parameters indexed by *: $x^* = x/H$ for instance, with $H = 0.25m$ the obstacle height. In order to consider turbulent event interaction with the free surface, experiments are achieved in Froude similitude. Furthermore, Reynolds number must be as high as achievable (see table I). As described in table I, the first case is based on an experimental representation of the Alderney Race. The second case is subsequently considered in the same experimental representation.

B. Description of the set-up

Two test cases, representative of different *in-situ* conditions, are considered, both are illustrated in figure 2 and described in table II along with measurement characteristics. The origin is taken in the centre of the bottom face of the obstacle.

	Scale	U_∞ [m/s]	Rugosity height H [m]	Depth D_e [m]	$R_e = \frac{HU_\infty}{\nu}$	$F_r = \frac{U_\infty}{\sqrt{gD_e}}$
Alderney Race	1	5	5	40	2.5×10^7	0,25
Flume tank	1/20	1	0,25	2	2.5×10^5	0,23

TABLE I: *in situ* and experimental conditions

First test case, denoted case A, consists in an experimental turbine positioned at $x^* = 16$ submitted to a strongly turbulent flow $I = 14\%$ with a uniform velocity profile at $1m/s$. No obstacle is positioned in the flow and the boundary layer developing in the tank never reaches the surface swept by the rotor [Ikhennicheu et al., 2017]. The turbine is positioned at mid-height of the tank, in the symmetry plane and rotating at a Tip Speed Ratio (TSR) of 4, with $TSR = \omega R/U_\infty$, $R = D/2$ the turbine radius and ω the rotation speed. TSR$= 4$ (TSR4) is the functioning point of the turbine, for which the power extraction is maximal [Mycek et al., 2014]. For this test case, only LDV (Laser Doppler Velocimetry) measurements are performed, first, synchronously $2D$ upstream of the turbine, hence at position $x^* = 16 - 2D/H = 10.4$ as it is commonly achieved for these type of set up [Gaurier et al., 2018a] and then close to the turbine position at $x^* = 15.8$ without the turbine.

The second test case, denoted case B, consists in the same turbine immersed in a wall-mounted cylinder wake. The cylinder has a squared section and its dimensions are $H \times 6H \times H$ ($H = 0.25m$). This obstacle wake is extensively described in [Ikhennicheu et al., 2019]. Both the obstacle and the turbine are at a 1:20 scale. Experiments are carried out for TSR4. The in-line distance between the turbine and the wall-mounted obstacle is $16H$ and the far upstream velocity is $U_\infty = 1m/s$. For this test case, the upstream turbulent intensity is low: $I = 1.5\%$. LDV measurements are performed synchronously $2D$ upstream of the turbine. PIV (Particle Image Velocimetry) measurements are also performed, the measurement plane is centred at the hub height in the vertical direction , aligned with blades root for the right part of the plane and in the symmetry plane of the tank in the transverse direction (see fig.4). Hence, as illustrated in figure 2(b) for this specific test case, both PIV and LDV are used, however measurements are not performed at the same time since the LDV probe immersed in the flow would induce vibrations on the PIV laser downstream.

For the two 2D laser velocimetry techniques, the tank is seeded with $10\mu m$ diameter silver coated glass particles. For the PIV measurements, a Nd-YAG Laser GEMINI-LIKE is used: power is $200mJ$ per probe and wavelength is $532nm$. It is synchronized with a Camera FLOWSENS EO-2M 1600pix $\times$ 1200pix that makes double images with

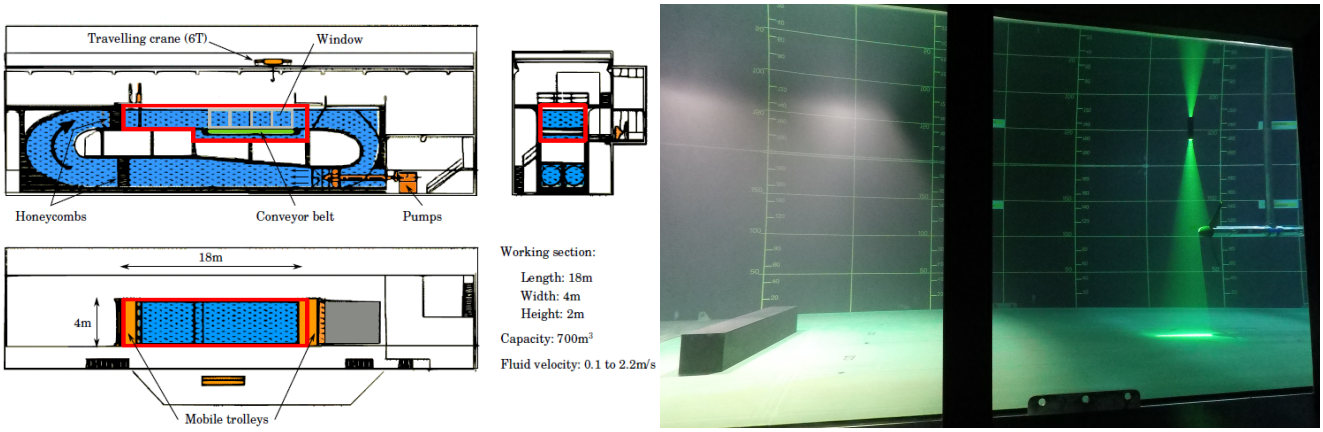

Fig. 1: Presentation of the wave and current circulating tank of IFREMER in Boulogne-sur-Mer (left) and picture of the experimental set-up with the wall-mounted cylinder and the PIV laser shooting in case B set-up (right).

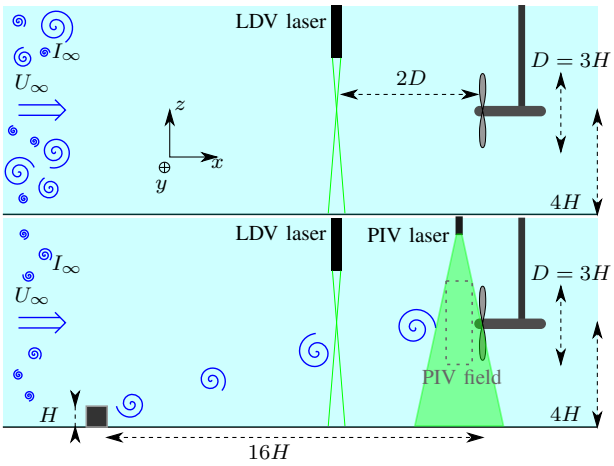

Fig. 2: Schematic representation of the two experimental set-ups: case A with $I = 14\%$ (top) and the case B with $I = 1.5\%$ and the presence of a wall-mounted cylinder (bottom). LDV measurements for case A, LDV and PIV measurements for case B.

a time step of 1600 μs. PIV acquisitions are made for $180s$, hence 2700 double images are taken with a $f_e = 15Hz$ acquisition frequency. The data are post processed with DYNAMIC STUDIO. Particles displacement is calculated using a Cross-Correlation [Meinhart et al., 1993]. Outliers are replaced with the Universal Outlier Detection [Westerweel and Scarano, 2005], example and precisions on that method can be found in [Ikhennicheu et al., 2019]. Measurements are performed in a $500\text{pix} \times 1200\text{pix} = 330mm \times 814mm$ plane with a spatial discretization of $11mm$.

The LDV measurements are performed using a 2D DANTEC FIBERFLOW system with wavelengths of 532 and $488nm$. With LDV measurements, the acquisition frequencies are not constant. They depend on when the particles are passing through the measurement volume and vary between $[100; 650]Hz$. Based on previous works performed in the tank [Duràn Medina et al., 2015], a re-sampling is performed using the mean sample rate of the dataset acquired. For the measurement techniques, uncertainty is estimated to be around 2% for LDV and 2.6% for PIV [Ikhennicheu et al., 2019].

In this study, a 3-bladed horizontal axis turbine model with $D = 725mm \simeq 3H$ diameter, recently developed at IFREMER [Gaurier et al., 2017], is used. The turbine model is equipped with 5-components blade root load-cells, measuring 2 forces and 3 moments for the 3 blades, in addition to torque and thrust transducers for the main rotation axis. Turbine parameters acquisition is synchronized with the PIV (or the LDV) measurements, and with a sampling frequency of $120Hz$.

Case	Obstacle	I_∞ [%]	Velocimeter	Probe position	f_e $[Hz]$	Duration $[min]$
A	None	14	LDV	$x^* = 15.8$	654	6
			LDV	$x^* = 10.4$	612	30
B	Cylinder	1.5	PIV	$x^* = 15.8$	15	3
			LDV	$x^* = 10.4$	208	6

TABLE II: Sum up of the 2 test cases and measurements performed. For a probe at $x^* = 10.4$, measurements are performed $2D = 5.6H$ upstream of the turbine and synchronized with it and for probe at $x^* = 15.8$, measurements are performed $0.2H$ upstream of the turbine position without its presence.

III. DETAILS OF THE INFLOW CONDITION

A. *Spatial description*

The upstream flow that impacts the turbine is described in this section. Velocity profiles are measured in the tank without the turbine at: $x^* = 15.8$ and compared in figure 3. For case A, the velocity profile is relatively uniform in the vertical direction. Standard deviation is high since

turbulence intensity equals 14%. Case B profile illustrates the extend of the cylinder wake. It presents a strong shear: the velocity difference between the top and the bottom position is $\Delta u = 0.23m/s$. Turbulence intensity is also very high at the bottom position where $I_{1D} \sim 20\%$ whereas the top position is less affected by the cylinder wake and the turbulence intensity is of the order of $I_{1D} \sim 5\%$. Compared to case A profile, the shear is higher for case B and the turbulence intensity is higher at the low position and lower at the top position. Case A flow is uniform, hence the velocity profile is the same at every streamwise position. For case B, due to the wake evolution and the vortex generation [Ikhennicheu et al., 2019] velocity differences are expected. Indeed at $(x^* = 15.8, z^* = 4)$, $U = 0.92 \pm 0.11m/s$ as opposed to measurements at $(x^* = 10.4, z^* = 4)$ where $U = 1.03 \pm 0.07m/s$ (see table III). Hence, for case B, average and fluctuating part are different depending on the streamwise position.

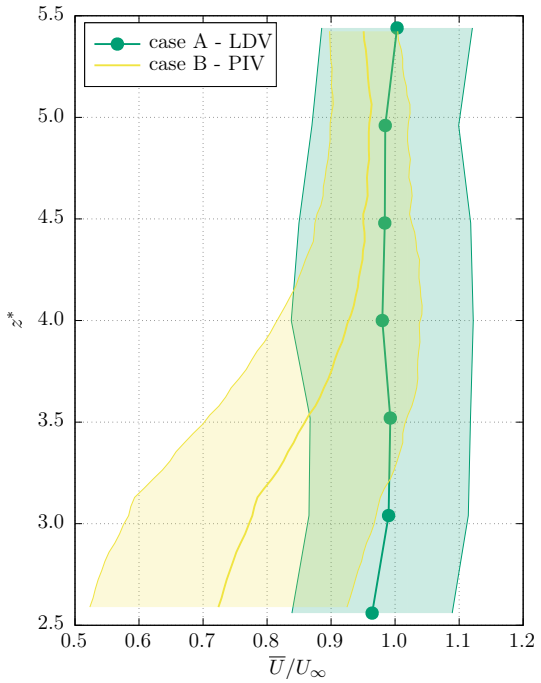

Fig. 3: Streamwise velocity $\overline{U}$ profiles with standard deviations for case A (LDV measurements) and B (PIV measurements) at $x^* = 15.8$, without the turbine. $[2.5 : 5.5]$ corresponds to the turbine diameter.

PIV measurements allow a 2D representation of the velocity field impacting the turbine, which is useful for vortex visualization. On figure 4, an example of vortex created in the cylinder wake is depicted before passing through the swept area. Such coherent structures properties are evaluated in [Ikhennicheu et al., 2018]: their radius in average: $0.2m$ and their circulation $-0.09m^2/s$.

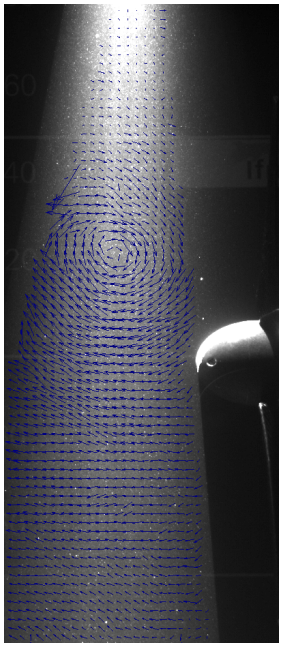

Fig. 4: Instantaneous fluctuating PIV field (u', w'), superimposed with a picture of the PIV laser shooting ahead of the turbine

B. Temporal and spectral description

Temporal signals are analysed for both test cases at the hub altitude $z^* = 4$ at $x^* = 10.4$. Experimental conditions for each test case are summed up in table II. Values of streamwise velocity at the selected point are evaluated in table III.

		Position	$\overline{U}$ $[m/s]$	$\sigma(u)$ $[m/s]$	I_{1D} $[\%]$
Case A	LDV	$10.4H$	0.98	0.13	13.2
Case A	LDV	$15.8H$	0.97	0.13	13.4
Case B	LDV	$10.4H$	1.03	0.07	7.1
Case B	PIV	$15.8H$	0.92	0.11	11

TABLE III: Velocity properties at hub height with measurement $2D$ upstream of the turbine $(x^* = 10.4)$ and close to the turbine $(x^* = 15.8)$

LDV allows a better temporal resolution and is preferred to PIV for this analysis. Figure 5 shows the velocity signals on a selected time range. For both test cases, velocity fluctuations range is $[0.4; 1.6]m/s$. For case A, fluctuations are in average larger $(\sigma(u_A) > \sigma(u_B))$ and some large scale fluctuations can be detected [Duràn Medina et al., 2017]. With the addition of the honeycomb for test case B, these lare scale strucutres are broken. However, large scale structures are created in the cylinder wake. They are due to Kelvin-Helmholtz instabilities developing behind the cylinder and interacting between each other to form large scale coherent turbulent events [Ikhennicheu et al., 2019]. Although the profile considered here is taken at $x^* = 10.4$, same type of structures will be detected at the turbine

position [Ikhennicheu et al., 2019]. Integral length scale can be evaluated using a method described in [Blackmore et al., 2016] with LDV measurements. It yields: $L_A = 0.39m$ [Duràn Medina et al., 2017] and $L_B = 0.29m$. Both are in the order of the turbine radius. Hence, large scale structures are detected for both cases. Their intensity is similar but their length scale is different.

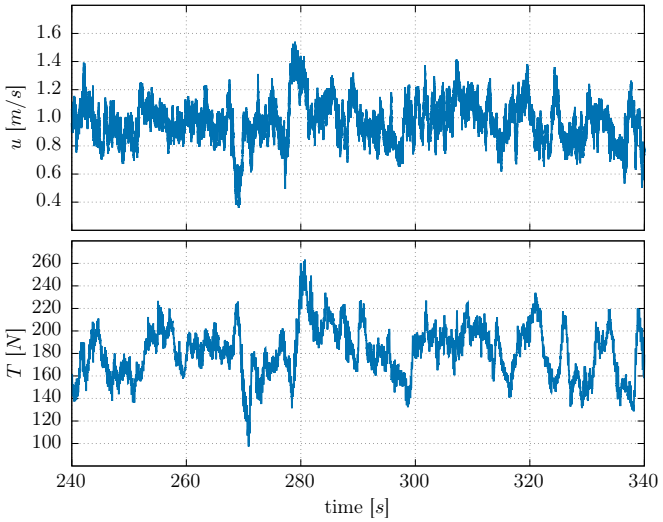

(a) U (top) and T (bottom) for case A

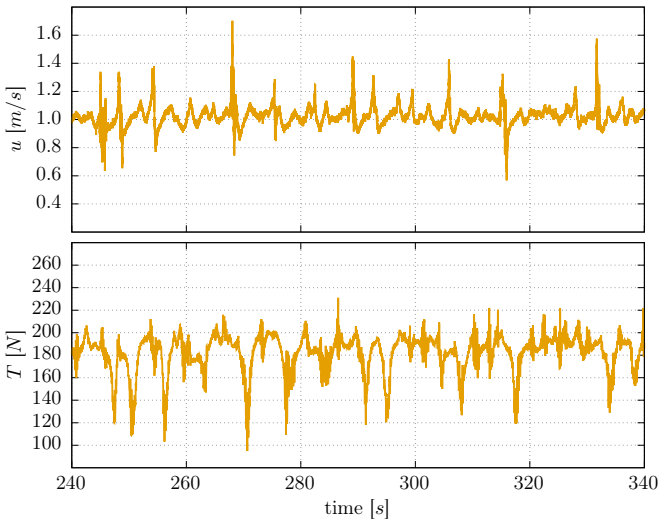

(b) U (top) and T (bottom) for case B

Fig. 5: Time history of streamwise velocity U and thrust T for case A (blue) and case B (yellow) with LDV measurements at $x^* = 10.4$, $z^* = 4$

Power Spectrum Densities (PSD) of the signals are plotted in figure 6. Beforehand, signals are cut into blocks, FFT (Fast Fourier Transform) is applied on every block and the result is averaged. For test case A (resp. B), blocks of 2^{15} elements (resp. 2^{12}) are performed. For both test cases, the spectra are in good adequacy with the $-5/3$ slope, a representation of the Richardson-Kolmogorov cascade of energetic transfer in turbulence [Pope, 2000]. The notable difference is the existence of a wide peak on case B spectrum around $f_s = 0.3Hz$. This peak is due to the periodic vortex shedding from the cylinder wake [Ikhennicheu et al., 2019]. Furthermore, the case A spectrum amplitude is higher than case B: at $f = 10Hz$, $S_{uuA} = 7 * 10^{-5}m^2/s$ and $S_{uuB} = 2 * 10^{-5}m^2/s$. That difference is due to the turbulence intensity difference.

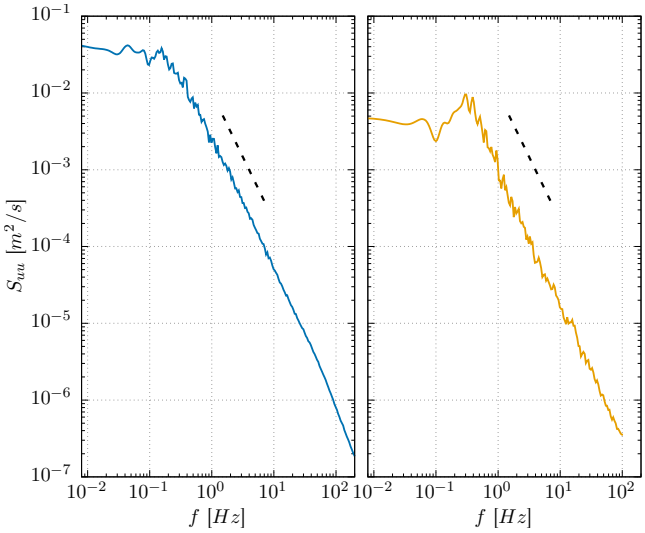

Fig. 6: PSD of u' for case A (left) and case B (right) with LDV measurements at $x^* = 10.4$, $z^* = 4$. Dotted line represent the $f^{-5/3}$ slope of the Richardson-Kolmogorov theory.

IV. Impact of flow variations on the turbine

The impact of the flow variations presented in the previous section on the turbine loads are studied. For test cases A, the velocity measured at $x^* = 10.4$ is representative enough (because there is no dissipation along the test section) to compare it to the turbine loads [Gaurier et al., 2018a]. For test case B, LDV measurements at $x^* = 10.4$ and PIV measurements at $x^* = 15.8$ are both compared to the load fluctuations.

A. Temporal analysis

Thrust fluctuations are illustrated in figure 5. Large scale velocity fluctuations detected on the velocity signals are also detected on the thrust signals for both cases. Thrust range is of the same order for both cases: from $100N$ to $250N$. In average $T_A = 179 \pm 21N$ and $T_B = 183 \pm 17N$. Thrust values are almost identical. Standard values are also close although velocity standard deviations are different by a factor of 2 ($0.07m/s$ compared to $0.13m/s$). An explanation will be proposed further in the paper. The power is also similar for both cases: $P_A = 83.7 \pm 19.0W$ and $P_B = 84.1 \pm 12.6W$.

Cross-Correlation ρ_{uT} between u' and T' is evaluated. It measures the similitude between two signals as a function of the time lag of one relative to the other. It is defined by equation 2.

$$\rho_{uT}(\tau) = \sum_{i=1}^{N_t} \frac{u'(t_i)T'(t_i+\tau)}{N_t} \tag{2}$$

ρ_{uT} is evaluated using LDV measurements for case A and both LDV and PIV measurements for case B. Curves are represented in figure 7. Comparing case A and case B using LDV measurement, it appears that case A shows a larger correlation ($\rho_{uT} = 0.65$ compared to $\rho_{uT} = 0.45$). Indeed, in case B, LDV is too upstream to capture all the fluctuations impacting the turbine due to the rising nature of the wake emitted vortices [Ikhennicheu et al., 2019]. For test case B, peak is maximal using close PIV measurements: $\rho_{uT} = 0.7$. Hence for case B, measurements close to the turbine are more accurate to correlate load fluctuations to velocity fluctuations. Indeed, there is a loss of correlation when the distance between the flow measurement point and the rotor increases. The correlation maximal value corresponds to the flow convection, in case A, the peak is at $\tau \sim -1.47s$ which is equal to $2D \times \overline{U}$.

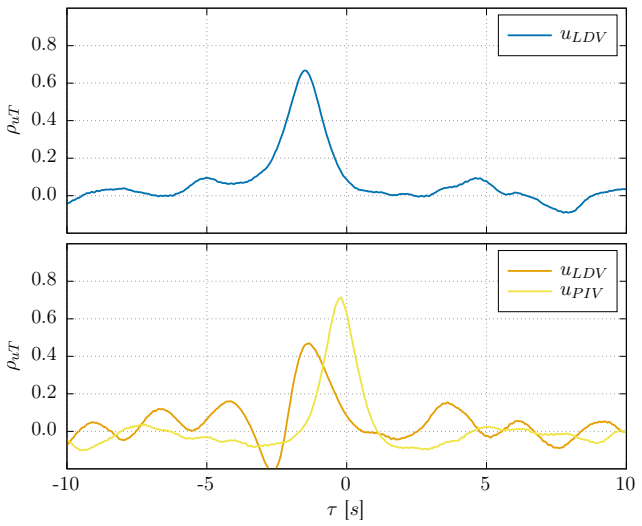

Fig. 7: Cross-correlation ρ_{uT} between the thrust and the velocity upstream of the turbine at $x^* = 10.4$ for LDV and $x^* = 15.8$ for PIV. Case A (top) and case B (bottom).

Using PIV measurements for case B, the cross-correlation calculations can be extended to every measurement point of the profile at $x^* = 15.8$ and not only at the mean rotor altitude. In figure 8, ρ_{uT} is evaluated for $z^* \in [2.5; 5.7]$ versus time lag. ρ_{uT} distribution shows a large correlation area ($max(\rho_{uT}) = 0.8$) below $z^* = 4.7$ and a small negative correlation area above that is too weak ($min(\rho_{uT}) = -0.4$) to be accounted for. That distribution means that turbulent events like the one illustrated in figure 4 induce a strong correlation between velocity and thrust fluctuations for $z^* < 4.7$. Such an analysis shows that a measurement at one specific point is not appropriate since data would be missing to grasp the whole mechanism. Hence, measurements on the full profile should be preferred.

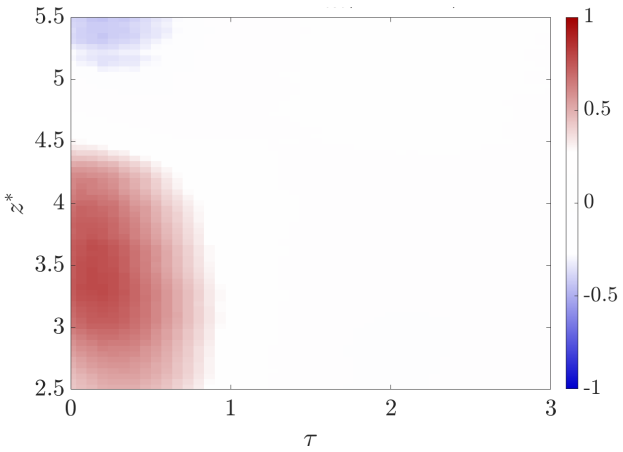

Fig. 8: Map of cross-correlation ρ_{uT} between the thrust T and the velocity upstream of the turbine U_z for $z^* \in [2.5; 5.7]$ at $x^* = 15.8$ for case B.

B. *Spectral analysis*

Spectral analysis is performed for the thrust signals. As for the velocity, signals of the thrust fluctuating component are cut into blocks of 2^{11} elements (resp. 2^{12}) for case A (resp. case B). Power Spectrum Densities are represented in figure 9. Curves follow a $-11/3$ slope that is also found in the work of [Chamorro2014] on a full scale horizontal wind turbine. They explain that the decay in the form of $f^{-11/3} = f^{-5/3}f^{-2}$ suggests a complex non-linear interaction between the loads and the energy density decay of the flow within the inertial range. On both spectra, a peak is detected at $f \sim 5Hz$ along with its harmonic at $f \sim 10Hz$. It is caused by the blade passing frequency equals to three times the turbine rotation frequency. Indeed, for TSR4 and with $D = 0.72$, $RPM = 105.4tr/min$ which yields in a rotation frequency of $f_r = 1.8Hz$, and $3f_r = 5.3Hz$. Spectra have a similar amplitude which seems logical since their standard deviation values are close. A peak at $f = f_s = 0.3Hz$ is slightly visible on case B spectrum. It is a sign that the structures shed in the cylinder wake are detected on the turbine loads.

Coherence between the thrust and the velocity C_{uT} is computed using equation 3. It shows the relation between two signals in the frequency domain. It is evaluated using the co-spectra of the signals considered. Here, coherence is evaluated using an FFT applied on blocks: the same as for PSD calculations for LDV and 2^9 elements are considered for PIV. Beforehand, the signal with the highest acquisition frequency is down-sampled to the same frequency as the other.

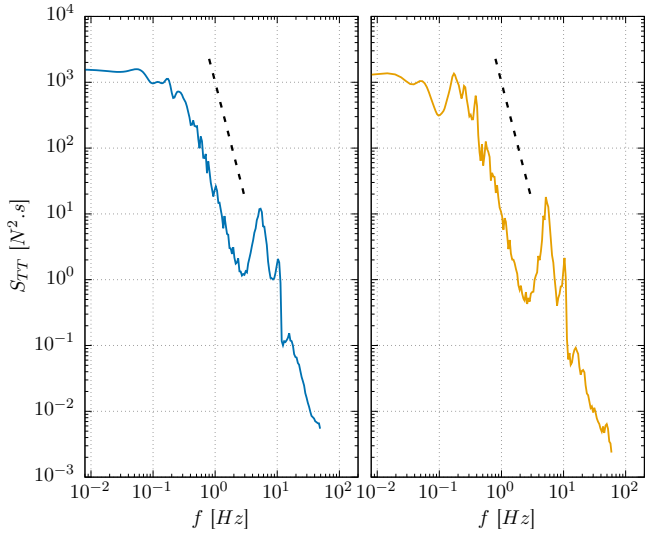

Fig. 9: PSD of the thrust T for case A (top) and case B (bottom) at $x^* = 10.4$ using LDV measurements. Dotted line represent a $f^{-11/3}$ slope.

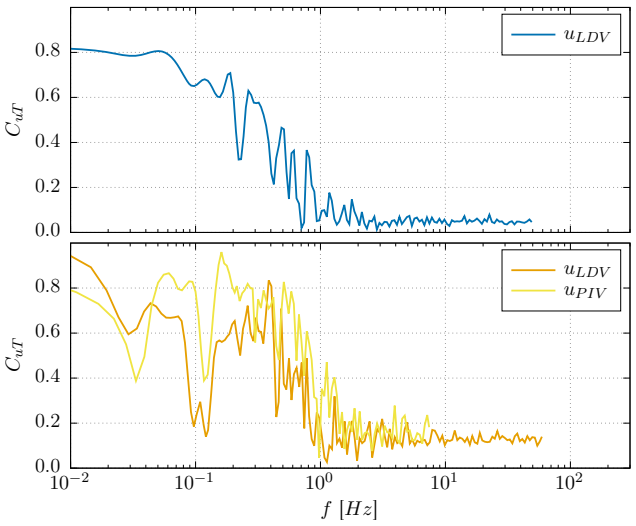

Fig. 10: Coherence C_{uT} between the thrust and the velocity upstream of the turbine at $x^* = 10.4$ for LDV and $x^* = 15.8$ for PIV. Case A (top) and case B (bottom).

$$C_{uT}^2(f) = \frac{|S_{uT}(f)|^2}{S_{uu}(f)S_{TT}(f)} \tag{3}$$

Coherence is evaluated for both cases in figure 10. First observation is that for both cases, coherence is close to 0 when $f > 1Hz$. Indeed, high frequency fluctuations, present on the case A velocity signal (figure 5) follow a $-5/3$ law whereas the thrust has a different behaviour with a $-11/3$ law. Turbine loads fluctuations are then decoupled from velocity fluctuations above $1Hz$. The critical frequency at which that phenomenon occurs is dependant on the turbine size (compared to the turbulence structures size) and the rotation velocity [Chamorro et al., 2014]. The decoupling between U and T at high frequencies might explain the closeness of T values for cases A and B (see section IV-A). Figure 10(b) illustrates the higher coherence at low frequencies ($f \in [10^{-1}; 10^{0}]$) for case B (u_{PIV}) compared to case A. At $0.5Hz$ the coherence is almost twice as high for case B. Large scale structures emitted from the cylinder at $f_s = 0.3Hz$ are within this range. These structures, organized and periodic, are transcribed onto the turbine loads hence the higher coherence in that frequency range. Another aspect is once again, that close PIV measurements are more coherent to the thrust compared to $2D$ upstream LDV measurements. Indeed, at $x^* = 10.4$, same structures type are detected although they might continue rising above the turbine and thus not be detected on the loads fluctuations.

Using PIV measurements for case B, the coherence calculations can be extended to every measurement point of the profile at $x^* = 15.8$. In figure 11, C_{uT} is evaluated for $z^* \in [2.5; 5.7]$ versus the frequency. The coherence map shows a good coherence for $f \in [10^{-1}; 10^{0}]$ at $z^* < 4.7$. It also illustrates that a coherence that drops at 0 at $1Hz$ is not always applicable. Indeed, for $z^* < 3$, the critical frequency is around $0.5Hz$.

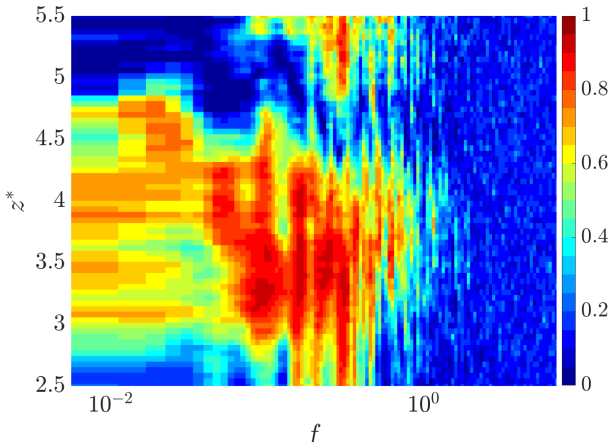

Fig. 11: Map of coherence C_{uT} between the thrust T and the velocity upstream of the turbine u_z for $z^* \in [2.5; 5.7]$ at $x^* = 15.8$ for case B.

C. Discussion on power coefficient calculation

Power evaluation usually leads to power coefficient C_P calculation using equation 4.

$$C_P = \frac{P}{\frac{1}{2}\rho S U^3} \tag{4}$$

where ρ is the water density, S the rotor area and U the velocity. Which velocity U should be considered?

In the literature, a measurement point $2D$ upstream of the turbine, performed simultaneously to the thrust acquisitions, is usually chosen [Germain et al., 2018, Gaurier et al., 2018a]. However, as it is explained earlier, in case B, velocity average value and energetic content is different depending on the streamwise position.

A solution could be to measure the velocity as close as possible and in synchronization with the turbine, at $x^* = 15.8$. However, the turbine presence perturbates the flow. Profiles with and without the turbine are presented in figure 12. The presence of the rotating turbine induces a strong velocity deficit (about 20% at the hub position) and an inflexion of the velocity profile shape. Indeed, the momentum theory shows that the flow speed should reduce from free-stream conditions far upstream of the turbine to the velocity incident at the rotor plane. Hence the turbine presence induces a velocity deficit that will strongly impact the C_P value. Measurements in the empty tank at the turbine position would then be the optimal option. However, loads measurements cannot be achieved synchronously and C_P would have to be normalized using a previously acquired velocity measurement which may lead to inaccurate results [Gaurier et al., 2018a].

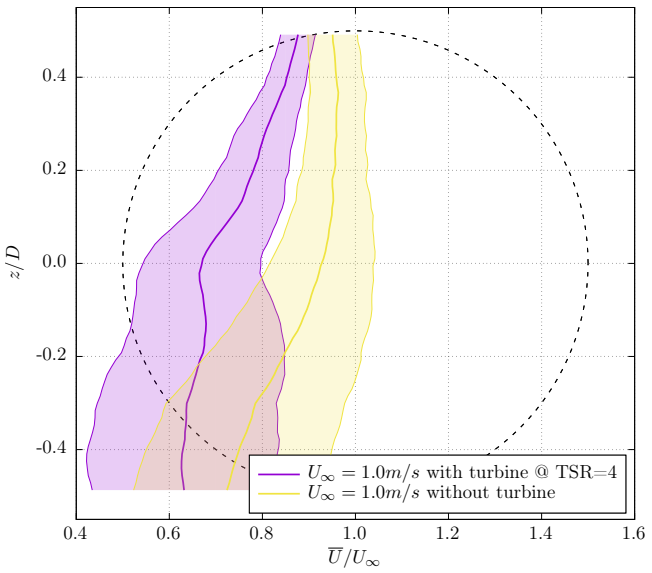

Fig. 12: Streamwise velocity $\overline{U}$ profiles with standard deviations for case B at $x^* = 15.8$, from PIV measurements

For comparison purposes, C_P values are evaluated using different flow velocity reference values and when it is achievable, C_P is evaluated instantaneously (meaning, at each times step, a $C_{p,i}$ is calculated and then C_p is evaluated as mean$(C_{p,i})$):

- Using upstream LDV measurements at ($x^* = 10.4$, $z^* = 4$): $\overline{U} = 1.03m/s$ and $C_P = 0.39$ (instantaneous calculations)
- Using PIV measurements at ($x^* = 15.8$, $z^* = 4$), without the turbine: $\overline{U} = 0.92m/s$ and $C_P = 0.47$
- Using PIV measurements at ($x^* = 15.8$, $z^* = 4$), with the rotating turbine: $\overline{U} = 0.67m/s$ and $C_P = 0.64$ (instantaneous calculations)
- Using PIV measurements on the whole profile, spatially averaged ($x^* = 15.8$), without the turbine: $\overline{U} = 0.89m/s$ and $C_P = 0.54$

All C_P values are different, $2D$ upstream LDV measurements might not be the best way to calculate C_P in this case. Also, taking measurement close to the rotating turbine yields into a abnormally elevated C_P. Further discussions on C_P evaluations are then required to give recommendations for protocol definition.

V. Conclusion

The turbulence presence in the inflow causes changes in a tidal turbine production and its structural fatigue. *In-situ*, high level of turbulence can be measured. In the present paper, two test cases are considered. First, a flow with high ambient turbulence (case A) and second, a low turbulence intensity flow with a wall-mounted cylinder producing a turbulent wake (case B). In both cases, an experimental turbine is disposed in the flow and within the cylinder wake for case B.

The two inflow conditions are first compared. Case A produces a uniform profile with an elevated turbulent intensity. Large turbulent structures exist within the flow although no specific frequency is detected on the spectrum. Case B presents a profile with a strong shear due to the cylinder wake. Spectral analysis shows a peak indicating a periodic vortex shedding from the cylinder wake. For both cases, the turbine thrust and power are in the same order of magnitude for the mean value and the standard deviation. Cross-correlation between the measured velocity and the thrust is evaluated. It is more elevated for case B. It also shows that, for case B, far upstream LDV measurements are less correlated than close PIV measurements. PIV measurements are used to draw a map of cross-correlation showing a correlation area for $z^* < 4.7$. Both thrust spectra show a peak at three times the turbine rotation frequency and, for case B, a peak at the vortex shedding frequency. Coherence around the shedding peak frequency is more elevated for case B.

The question of the velocity used for C_P computation is asked. In case A, upstream simultaneous measurements are known to be valid. For case B, due to the evolving nature of the cylinder wake energetic content, measurements at the turbine positions must be carried out. However, simultaneous close measurements are not achievable.

To conclude, this paper compares two types of incoming turbulent profiles. Even though the turbine thrust and power values are similar for both cases, the turbulent structures embedded in the flow are different. For case B, periodic events and a sheared profile may be the most critical for the turbine

fatigue. Due to its more organized nature, case B is also the case for which turbine loads are more correlated to the inflow. Authors also underline the limitation of the usual upstream LDV measurement point. This set-up is not applicable in the specific case of an obstacle wake. The cross-correlation and coherence maps will be further developed using loads on each blade and the vertical velocity. 2D PIV planes can also be used to correlate a vortex structure passing to loads variations. Experiments were also carried out at TSR0 and will be used to better understand the loads distribution. Authors also intend to continue discussing the more adapted velocity to be taken into account for power coefficient evaluation.

ACKNOWLEDGEMENT

The authors acknowledge the financial support of IFREMER and the Hauts-de-France Regional Council for these PhD studies. This work benefits from a French State grant managed by the National Research Agency under the Investments for the Future program bearing the reference ANR-10-IEED-0006-11. MET-CERTIFIED is receiving funding from the Interreg 2 Seas programme 2014-2020, co-funded by the European Regional Development Fund under subsidy contract No 2S01-020. We are most grateful to Thomas Bacchetti and Inès Belarbi for their assistance and precious advices.

REFERENCES

[Best, 2005] Best, J. (2005). The fluid dynamics of river dunes: A review and some future research directions. *J. Geophys. Res.*, 110.

[Blackmore et al., 2016] Blackmore, T., Myers, L. E., and Bahaj, A. S. (2016). Effects of turbulence on tidal turbines: Implications to performance, blade loads, and condition monitoring. *International Journal of Marine Energy*, 14:1 – 26.

[Chamorro et al., 2015] Chamorro, L., Hill, C., Neary, V., Gunawan, B., Arndt, R., and Sotiropoulos, F. (2015). Effects of energetic coherent motions on the power and wake of an axial-flow turbine. *Phys. Fluid*, 27:055104.

[Chamorro et al., 2014] Chamorro, L., Lee, S.-J., Olsen, D., Milliren, C., Marr, J., Arndt, R., and Sotiropoulos, F. (2014). Turbulence effects on a full-scale 2.5 mw horizontal-axis wind turbine under neutrally stratified conditions. *Wind Energ.*, 18:339–349.

[Davies et al., 2013] Davies, P., Germain, G., Gaurier, B., Boisseau, A., and Perreux, D. (2013). Evaluation of the durability of composite tidal turbine blades. *Phil. Trans. R. Soc. A.*, 371:20120187.

[Diabil et al., 2017] Diabil, H., Li, X., and Abdalla, I. E. (2017). Coherent structures and flow topology of transitional separated-reattached flow over two and three dimensional geometrical shapes. *Mathematical Methods and Computational Techniques in Science and Engineering-* AIP *Conference proceedings*, 020019.

[Duràn Medina et al., 2015] Duràn Medina, O., Schmitt, F., Calif, R., Germain, G., and Gaurier, B. (2015). Correlation between synchronised power and flow measurements, a way to characterize turbulent effects on a marine current turbine. *Proceedings of the 11th European Wave and Tidal Energy Conference, Nantes, France*.

[Duràn Medina et al., 2017] Duràn Medina, O., Schmitt, F., Calif, R., Germain, G., and Gaurier, B. (2017). Turbulence analysis and multiscale correlations between synchronized flow velocity and marine turbine power production. *Renew. Energ.*, 112:314–327.

[Gaurier et al., 2017] Gaurier, B., Germain, G., and Facq, J.-V. (2017). Experimental study of the Marine Current Turbine behaviour submitted to macro-particle impacts. *Proceedings of the 12th European Wave and Tidal Energy Conference, Cork, Ireland*.

[Gaurier et al., 2018a] Gaurier, B., Germain, G., and Pinon, G. (2018a). How to correctly measure turbulent upstream flow for marine current turbine performances evaluation? *Proceedings of the Renewable Energy Conference, Lisboa, Portugal*.

[Gaurier et al., 2018b] Gaurier, B., Ikhennicheu, M., Druault, P., Germain, G., Facqu, J.-V., and Pinon, G. (2018b). Experimental study of the wake of a wide wall-mounted obstacle on the behaviour of a marine current turbine. *Proceedings of the 16th Journée de l'Hydrodynamique, Marseille, France*.

[Germain et al., 2018] Germain, G., Gaurier, B., Harrold, M., Ikhennicheu, M., Scheijgrond, P., Southall, A., and Trasch, M. (2018). Protocols for testing marine current energy converters in controlled conditions. where are we in 2018 ? *Proceedings of the 4th Asian Wave and Tidal Energy Conference, Taipei, Taiwan*.

[Ikhennicheu et al., 2017] Ikhennicheu, M., Druault, P., Gaurier, B., and Germain, G. (2017). An experimental study of influence of bathymetry on turbulence at a tidal stream site. *Proceedings of the 12th European Wave and Tidal Energy Conference, Cork, Ireland.*

[Ikhennicheu et al., 2018] Ikhennicheu, M., Gaurier, B., Druault, P., and Germain, G. (2018). Experimental analysis of the floor inclination effect on the turbulent wake developing behind a wall mounted cube. *Eur. J. Mech. B/Fluid*, 72:340–352.

[Ikhennicheu et al., 2019] Ikhennicheu, M., Germain, G., Druault, P., and Gaurier, B. (2019). Experimental study of coherent flow structures past a wall-mounted square cylinder. *Under Review*.

[Kelley et al., 2005] Kelley, N., Jonkman, B., Bialasiewicz, J., Scott, G., and Redmond, L. (2005). Impact of coherent turbulence on wind turbine aeroelastic response and its simulation. *Windpower 2005 Conference Proceedings, Denver, Colorado.*, DC: American Wind Energy Association; Content Management Corp. 22 pp.; NREL Report No. CP-500-40187.

[Meinhart et al., 1993] Meinhart, C., Prasad, A., and Adrian, R. (1993). A parallel digital processor system for particle image velocimetry. *Meas. Sci. Technol.*, 4:619–626.

[Mycek et al., 2014] Mycek, P., Gaurier, B., Germain, G., Pinon, G., and Rivolaen, E. (2014). Experimental study of the turbulence intensity effects on marine current turbines behaviour. Part I: One single turbine. *Renew. Energ.*, 66:729–746.

[Myers and Bahaj, 2005] Myers, L. and Bahaj, A. (2005). Simulated electrical power potential harnessed by marine current turbine arrays in the Alderney Race. *Renew. Energ.*, 30:1713–1731.

[Pope, 2000] Pope, S. (2000). Turbulent flows. *Cambridge University Press, Cambridge*.

[Sellar et al., 2018] Sellar, B., Wakelam, G., Sutherland, D., Ingram, D., and Venugopal, V. (2018). Characterisation of tidal flows at the european marine energy center in the absence of ocean waves. *Energ.*, 11:176.

[Thomson et al., 2012] Thomson, J., Polagye, B., Durgesh, V., and Richmond, M. (2012). Measurements of turbulence at two tidal energy sites in puget sound, WA. *IEEE J. OCEANIC ENG.*, 37.

[Westerweel and Scarano, 2005] Westerweel, J. and Scarano, F. (2005). Universal outlier detection for PIV data. *Exp. Fluids*, 39:1096–1100.